Original Papers

Triangular-wave controlled amplitude-modulated flow analysis for extending dynamic range to saturated signals

Hideji TANAKA,*,**,† Riona WADA,** Masatoshi YANASE,** Erina TOMIYAMA,** Akira OHBUCHI,*** Keiro HIGUCHI,**** and Masaki TAKEUCHI*,**

** Institute of Biomedical Sciences, Tokushima University, 1-78-1 Shomachi, Tokushima 770-8505, Japan*

*** Faculty of Pharmaceutical Sciences, Tokushima University, 1-78-1 Shomachi, Tokushima 770-8505, Japan*

***** Graduate School of Technology, Industrial and Social Sciences, Tokushima University, 2-1 Minami-Josanjima, Tokushima 770-8506, Japan*

**** Ogawa & Co., Ltd., 3-1-25 Hiocho, Nada-ku, Kobe 657-0029, Japan*

† To whom correspondence should be addressed.

E-mail: h.tanaka@tokushima-u.ac.jp

Abstract

We have applied our amplitude-modulated flow analysis concept to extend the dynamic range to saturated analytical signals. Sample solution, the flow rate F_S of which is periodically varied with a triangular control signal V_c, is merged with a reagent solution delivered at a constant flow rate F_R. While the total flow rate F_T is kept constant, a diluent with $F_T - (F_S + F_R)$ flow rate is aspirated from the third channel. The analytical signal V_d obtained downstream is processed by fast Fourier transform to obtain the amplitudes of the wave components in V_d. When the sample concentration C_S is low, V_d shows a triangular profile like V_c; the sum of the amplitudes ΣA is proportional to C_S. When C_S is high, V_d shows a trapezoidal profile because of the V_d saturation. A linear calibration curve can also be obtained for such saturated signals by plotting $C_S\Sigma A$ against C_S. The proof of the concept is validated by applying it to spectrophotometric determinations of a dye (Methylene Blue) and colored complexes of Fe^{2+}–phenanthroline and Fe^{3+}–Tiron.

Keywords: Amplitude modulated flow analysis, flow rate modulation, triangular-wave control, fast Fourier transform, saturated signal.

Introduction

Amplitude-modulated multiplexed flow analysis (AMMFA), proposed by Tanaka *et al*. [1], is a flow-based analysis for multiple sample analysis. The information on samples are amplitude-modulated by periodically varying their flow rates at different frequencies. The downstream analytical signal is processed by fast Fourier transform (FFT). Air-segmented AMMFA [2-5] and internal standard AMMFA [6] were further developed to improve the measurements' sensitivity and robustness, respectively. AMMFA could also be applied to determing multiple analytes in a single sample [3,7].

In the present paper, we propose a triangular-wave controlled amplitude-modulated flow analysis for extending the dynamic range to saturated signals. The flow rate of the sample solution is periodically and triangularly varied. After it is merged with a color reagent solution, the absorbance of the colored product is measured downstream and analyzed by FFT. Analytical signals show a triangular profile when the sample concentration is low. In this case, ΣA is proportional to C_S, where ΣA and C_S mean the sum of amplitudes obtained by FFT and the analyte concentration, respectively. On the other hand, the analytical signals show a trapezoidal profile when the concentration is high because of the analytical signals' saturation due to the detector's upper measurable limit or the reagent shortage. A linear calibration curve can also be obtained by plotting $C_S\Sigma A$ against C_S for the saturated signals. The present paper will focus on the proof of the concept by using Methylene Blue and iron complexes.

Lisec *et al*. [8] reconstructed a GC-MS peak from saturated signals based on isotope ratio and Gaussian distribution function. The dynamic range was extended to higher concentrations by more than one order of magnitude. Kadjo *et al*. [9] reported a width-based quantitation paradigm for chromatographic peaks. The peaks' leading and tailing halves were modeled as two different independent Gaussian distribution functions. They applied the paradigm to

clipped/truncated ion chromatographic peaks caused by nonlinear or saturated detector responses [10]. The present amplitude-modulated concept would be an alternative approach for high concentration sample analysis.

Experimental

Reagents

Methylene Blue (MB) and ammonium iron(III) sulfate dodecahydrate ($FeNH_4(SO_4)_2 \cdot 12H_2O$) were purchased from Fujifilm Wako Chemicals (Osaka). Ammonium iron(II) sulfate hexahydrate ($Fe(NH_4)_2(SO_4)_2 \cdot 6H_2O$) was purchased from Nacalai Tesque (Kyoto). 1,10-Phenanthroline monohydrate, Tiron (4,5-dihydroxy-1,3-benzenedisulfonic acid disodium salt), acetic acid (> 99.7%), and sodium acetate trihydrate were purchased from Kanto Chemicals (Tokyo). Other reagents used were respectively purchased from one of the manufactures mentioned above. All the reagents were of analytical reagent grade and were used without further purification. Sartorius Arium 611 DI grade deionized water (resistivity, 18.2 MΩ cm) was used throughout.

Flow system

Figures 1 show the flow system fabricated in the present study. The system was of three-channel manifold unless otherwise stated. The flow rate of sample solution S was varied using a peristaltic pump P_1 (Gilson Minipuls 3, MP-2, USA) controlled by a triangular control signal V_c supplied from a signal generator SG (NF Corp. WF1974, Japan). Color reagent solution CR was delivered with P_2 (the same model as P_1) at a constant flow rate, while the total flow rate was held constant with P_3 (Rainin Dynamax RP-1, USA). PharMed tubing with 0.51 mm i.d. was used for P_1 – P_3 as pump tubes. Water was aspirated from the third channel to

make up for the constant total flow rate. The merged solution was allowed to flow upwards in a lab-made quartz cell (optical path length, 1 mm) set in a UV/Vis spectrophotometer D (Shimadzu SPD-10AV$_{VP,}$ Japan) so that accidentally introduced air bubbles could be easily flushed away. There, the relative absorbance of a narrow solution region was measured. The analytical wavelengths for MB, Fe^{2+}, and Fe^{3+} were 660, 510, and 660 nm, respectively. The detector output signals V_d (0.5 absorbance unit / V) and V_c were quantized by an A/D-D/A converter (Contec AIO-160802GY-USB, Japan). The resulting digital data were acquired into a laptop computer PC (mouse m-book E410BN, Japan) in Microsoft Excel format.

Software

An in-house program written in Microsoft Visual Basic .NET was used to acquire signals, perform FFT calculations, and display the results automatically. The FFT algorithm was referred to in a book authored by Nakamura [11]. Table 1 shows the typical analytical parameters. The V_c was of a triangular-wave profile with the range of 0 − 5 V and the period of 60 s. This period was set as the FFT window's time length. The V_d was acquired at the sampling frequency of 17.06667 Hz. Sixteen data in the window (*i.e.*, every sixty-fourth 16 points) were used for FFT computation, according to the discrete Fourier transform formula:

$$X_k = \frac{1}{N}\sum_{n=0}^{N-1} x_n \ \exp\left(-j\frac{2n\pi k}{N}\right), \quad (1)$$

where N is the number of data for the FFT computation (*i.e.*, 16), and j is the imaginary number. Because 16 data were used for the FFT computation, up to the eighth harmonic wave component's amplitude could be obtained based on the sampling theorem [12]. The X_0 corresponds to the direct current component in V_d; $2|X_1|$, $2|X_2|$…$2|X_7|$, and $|X_8|$ correspond to the amplitudes of the fundamental wave component A_1, the second harmonic wave component A_2

…the seventh harmonic wave component A_7, and the eighth harmonic wave component A_8, respectively. The FFT computation is carried out in real-time using a new 16 data set at regular intervals (1.875 s) by shifting the FFT window.

Principle

Figure 2 shows the schematic diagram of the present concept. The V_c, which controls the sample flow rate and thus determines the analyte concentration at the confluence point in the manifold, is varied triangularly with a period of T. The corresponding analytical signal V_d is obtained downstream. Therefore, there is a delay (t_{lag}) in the phase between V_c and V_d.

When the sample concentration C_S is low (Fig. 2(A)), V_d shows a triangular profile like V_c. The slope of V_d is proportional to C_S; that is, the slope is aC_S or $-aC_S$ for the upward and downward V_d, respectively, where a is a proportional constant. The a is proportional to the V_c scan rate, dV_c/dt, and molar absorptivity (in the case of absorbance measurement) and inversely proportional to the total flow rate. Based on the nature of the periodic signal and Fourier transform, the relationship between A_n (n = 1, 2, 3…) and C_S can be expressed only with a cosine term by setting t_a and t_b in Fig. 2(A) as time 0 and T, respectively.

$$A_n = \frac{aC_S T}{n^2\pi^2} - \frac{aC_S T}{n^2\pi^2}\cos n\pi \qquad (2)$$

A detailed derivation process for Eq. (2) is described in "Derivation of Eq. (2)" in Supporting Information. The A_n is 0 or $2aC_ST/(n^2\pi^2)$ when n is an even or odd number, respectively. Therefore, the following relationship is obtained between the sum of the amplitudes (ΣA) and C_S using a mathematical formula of $\Sigma\{1/(2k-1)^2\} = \pi^2/8$ [13].

$$\Sigma A = \Sigma\left\{\frac{aC_S T}{n^2\pi^2} - \frac{aC_S T}{n^2\pi^2}\cos n\pi\right\} = \frac{2aC_S T}{\pi^2}\left(\frac{1}{1^2} + \frac{1}{3^2} + \frac{1}{5^2} + \ldots\right) = \frac{2aC_S T}{\pi^2}\frac{\pi^2}{8}$$
$$= \frac{aC_S T}{4} \quad (3)$$

Eq. (3) indicates that ΣA is proportional to C_S.

When C_S becomes high (Fig. 2(B)), V_d is saturated due to the instrument's measurable upper limit or excess analyte to the reagent. This leads to a trapezoidal V_d profile with an upper limit L. Similar to the derivation of Eq. (2), A_n is also expressed only by a cosine term,

$$A_n = \frac{aC_S T}{n^2\pi^2} - \frac{aC_S T}{n^2\pi^2}\cos\frac{2n\pi L}{aC_S T} \quad (4)$$

A detailed derivation process for Eq. (4) is described in "Derivation of Eq. (4)" in Supporting Information. Therefore, the following relationship is derived for ΣA using mathematical formulae of $\Sigma(1/n^2) = \pi^2/6$ and $-\frac{1}{\pi^2}\Sigma\frac{cos\ 2n\pi x}{n^2} = x - x^2 - \frac{1}{6}$, when $0 \leq x \leq 1$ [13].

$$\Sigma A = \Sigma\left\{\frac{aC_S T}{n^2\pi^2} - \frac{aC_S T}{n^2\pi^2}\cos\frac{2n\pi L}{aC_S T}\right\} = \frac{aC_S T}{\pi^2}\Sigma\frac{1}{n^2} + aC_S T\left\{-\frac{1}{\pi^2}\Sigma\frac{\cos\frac{2n\pi L}{aC_S T}}{n^2}\right\}$$
$$= \frac{aC_S T}{\pi^2}\frac{\pi^2}{6} + aC_S T\left\{\frac{L}{aC_S T} - \frac{L^2}{(aC_S T)^2} - \frac{1}{6}\right\}$$
$$= L - \frac{L^2}{aC_S T} \quad (5)$$

A more detailed derivation process for Eq. (5) is described in "Derivation of Eq. (5)" in Supporting Information. Therefore, ΣA is inversely proportional to C_S. By multiplying both sides of Eq. (5) by C_S, a linear function of C_S is obtained.

$$C_S\,\Sigma A = LC_S - \frac{L^2}{aT} \quad (6)$$

Eq. (6) means that $C_S \Sigma A$ is proportional to C_S.

Results and Discussion

Concept validation using a dye solution

Aqueous solutions of Methylene Blue (MB) were used as samples because they needed no color reaction, making the concept validation easier. Figures 3(A) and (B) show V_c and V_d for the MB concentrations C_{MB} of 20 and 70 mg dm^{-3}, respectively. The V_d values are the moving average of 11 raw values. The t_{lag} estimated from the delay of the raw V_d from V_c is 12.4 s.

When C_{MB} was low (Fig. 3(A)), V_d showed a triangular profile. Contrary to the theoretical profile shown in Fig. 2(A), V_d did not reach 0 V. This is attributed to the axial dispersion of MB caused by diffusion and convection in the conduit. When C_{MB} was high (Fig. 3(B)), V_d reached the detector's upper limit (1.029 V), resulting in a trapezoidal profile. Figures 3(C) and (D) show amplitudes ($A_1 - A_8$) and their sum (ΣA) for respective V_d. The start of FFT computation needed to wait for 120 s until a complete data set for one FFT window was acquired. The $A_2 - A_8$ values in Fig. 3(C) and the $A_4 - A_8$ values in Fig. 3(D) were too small to be distinguished from each other. Therefore, the numerical data for Figs. 3(C) and (D) are listed in Table S1 (Supporting Information).

Figure 4(A) shows V_d in two periods (*i.e.*, 240 s) for various C_{MB}, where signals are superimposed to coincide in the phase. It shows that the V_d profile became trapezoidal when C_{MB} was higher than *ca*. 40 mg dm^{-3}. Figure 4(B) shows the plots based on Eqs. (3) and (6), respectively. In the range of 0 − 30 mg dm^{-3} C_{MB}, ΣA was proportional to C_{MB} (ΣA = 0.0130 C_{MB} + 0.0153, r^2 = 0.996), as expected by Eq. (3). The limit of detection (3.3σ) was 2.69 mg dm^{-3}. In the high C_{MB} range (40 – 90 mg dm^{-3}), linear relationship of C_{MB} ΣA =

0.6701 C_{MB} – 6.6791 (r^2 = 0.997) was obtained based on Eq. (6). These results indicate that the present method can quantify the analyte even if the analytical signals are saturated. That is, measure a sample solution whose C_{MB} is unknown, obtain its ΣA, and substitute it into either of the calibration curves. When the solution gives an unsaturated triangular V_d profile, C_{MB} is determined by the former calibration curve (C_{MB} = (ΣA – 0.0153)/0.0130); when the solution gives a saturated trapezoidal V_d profile, C_{MB} is determined from the latter calibration curve (C_{MB} = −6.6791(ΣA – 0.6701)). However, even higher C_{MB} (*i.e.*, 100 mg dm^{-3}) seemed inappropriate because its C_{MB} ΣA deviated from the linear relationship, presumably because of its large axial dispersion.

Linear relationships for the trapezoidal signal profile can also be obtained by plotting ΣA against C_{MB}^{-1} or $(C_{MB}\Sigma A)^{-1}$ against ΣA^{-1}, as respectively expressed by Eqs. (7) and (8).

$$\Sigma A = -\frac{L^2}{aT}\frac{1}{C_{MB}} + L \quad (7)$$

$$\frac{1}{C_{MB}\Sigma A} = \frac{aT}{L}\frac{1}{\Sigma A} - \frac{aT}{L^2} \quad (8)$$

Figure 4(C) shows the plot based on Eq. (7), for example; ΣA = −7.5758C_{MB}^{-1} + 0.6844 (r^2 = 0.929). However, we do not adopt these equations because they are not the function of C_{MB} but the functions of C_{MB}^{-1} and ΣA^{-1}, respectively. In addition, the data at C_{MB} = 0 cannot be used because C_{MB} is in the dominators in Eqs. (7) and (8).

It should be mentioned that ΣA in Figs. 3 and 4 was the sum of $A_1 - A_8$ in contrast to that in Eqs. (3), (5), and (6) was the sum of $A_1 - A_\infty$. However, the former could be regarded as the approximation of the latter because the higher harmonic wave component's amplitudes came to be trivial as its order increased (See Figs. 3(C), (D) and Table S1).

As a reference, MB was measured by a conventional FIA using the manifold shown in Fig. S3(A); the obtained signals are shown in Fig. S3(B) (Supporting Information). The signal became saturated at *ca*. 45 mg dm^{-3}, meaning that MB cannot be quantified above this concentration.

Concept validation by colorimetry

o-Phenanthroline spectrophotometry for Fe^{2+} was adopted because the stable colored Fe^{2+} complex was produced rapidly and stoichiometrically. The color reagent was 40 mmol dm^{-3} *o*-Phen in 0.9 mol dm^{-3} acetate buffer (pH 4.6). Figure S4 (Supporting Information) shows the effects of control period (A), reaction temperature (B), and reaction coil length (C) on ΣA. The lower the concentration gradient is, the lesser the axial dispersion in the conduit becomes, as pointed out by Kurokawa *et al*. [14] Therefore, amplitude damping was suppressed, and hence ΣA increased with an increase in the period (Fig. S4(A)). Such effect was not so significant when the period was longer than 60 s. By taking the sample throughput into account, 60 s was selected as the control period because sample concentration should be invariable for at least one FFT window. The reaction temperature and coil length did not have a significant effect on ΣA (Figs. S4(B) and (C), respectively). Therefore, 50 °C and 50 cm were selected respectively because these conditions seemed enough for the color reaction.

Figure 5(A) shows the plots based on Eqs. (3) and (6). The linear regression lines for C_{Fe2+} = 0 – 0.5 mmol dm^{-3} and C_{Fe2+} = 0.7 – 1.2 mmol dm^{-3}, respectively, are as follows:

$$\Sigma A = 0.8236\ C_{Fe2+} + 0.0062,\ r^2 = 1.000 \quad (9)$$

$$C_{Fe2+}\Sigma A = 0.6866\ C_{Fe2+} - 0.0701,\ r^2 = 0.993 \quad (10)$$

The LOD (3.3σ) obtained from Eq. (9) was 0.046 mmol dm^{-3}. If a sample with a concentration

of 1.2 mmol dm^{-3} Fe^{2+}, the present method's upper measurable limit, is analyzed by an official method (JIS. Quantification range: 20 − 500 μg / 100 cm^3) [15], the sample volume should be less than 7.46 cm^3 for the final volume of 100 cm^3.

The present method was also examined by applying it to Tiron spectrophotometry for Fe^{3+} determination. Analytical conditions were referred to the report by Kuroda *et al*. [16] A 10.5 mmol dm^{-3} Tiron in 0.15 mol dm^{-3} acetate buffer (pH 4.5) was used as a color reagent. The composition of Fe^{3+}−Tiron complex at pH 4.5 was determined by a molar ratio method (Fig. S5 in Supporting Information) because there seems to be some discrepancy in the complex composition (1 : 1 [17], 1 : 2 [18], both of them [19]) among the literature. The composition determined was 1:1, which was agreed with the result from a continuous variation method by Harvey and Manning [17]. The calibration curves based on Eqs. (3) and (6) are shown in Fig. 5B, respectively, showing good linearity for both low and high C_{Fe3+} ranges, as expected: ΣA = 0.1114 C_{Fe3+} + 0.0049 (r^2 = 0.997) with LOD of 0.062 mmol dm^{-3} for 0 – 1.5 mmol dm^{-3} Fe^{3+} and $C_{Fe3+}\Sigma A$ = 0.33123 C_{Fe3+} − 0.2373 (r^2 = 0.9994) for 2 − 4 mmol dm^{-3} Fe^{3+}.

Reduction of reagent consumption

The present concept was applied to the case where V_d saturates due to the reagent shortage. Figure S6 (Supporting information) shows the results of preliminary experiments carried out under low *o*-Phen concentration (C_{Phen}), where $C_{Fe2+}\Sigma A$ is plotted against C_{Fe2+} in the trapezoidal V_d region. It shows that the measurable range shifted towards lower C_{Fe2+} as C_{Phen} decreased. At 2 mmol dm^{-3} *o*-Phen, $C_{Fe2+}\Sigma A$ increased with C_{Fe2+} when C_{Fe2+} was lower 0.3 mmol dm^{-3}. Therefore, calibration curves for Fe^{2+} were prepared more precisely for this range with 2 mmol dm^{-3} *o*-Phen. Fig. S7 (Supporting Information) are the obtained calibration curves: ΣA = 0.6509 C_{Fe2+} + 0.0049 (r^2 = 0.999) with 0.018 mmol dm^{-3} LOD (3.3σ) for 0 – 0.08 mmol dm^{-3} Fe^{2+} that gave triangular V_d profiles; $C_{Fe2+}\Sigma A$ = 0.1220 C_{Fe2+} − 0.0264 (r^2 = 0.991)

for 0.1 – 0.2 mmol dm^{-3} Fe^{2+} that gave trapezoidal V_d profiles. The border of the two regions was agreed with the theoretical value of 0.095 mmol dm^{-3} (= C_{Phen} × (*o*-Phen flow rate) / (maximum Fe^{2+} flow rate) × 1/3). These results suggest that the present concept is applicable to the case where V_d saturates due to the reagent shortage. This feature is effective for reducing reagent consumption. *o*-Phen consumption per measurement (60 s) was 0.00026 mmol, which was 0.94% of that of the official method (batch method; final volume, 100 cm^3). [15] Kadjo *et al*. [10] also pointed out that their width-based quantification paradigm for saturated analytical signals effectively minimized added reagent. However, at even higher C_{Fe2+} (*i.e*., 0.25 and 0.3 mmol dm^{-3}), the amplitude damping through the axial dispersion caused the deviation of the plots from the linear regression line. Up to 50 mmol dm^{-3} Mg^{2+} and 500 mmol dm^{-3} Ca^{2+} were tolerable for 0.05 mmol dm^{-3} Fe^{2+} determination.

Figure S8 (Supporting Information) shows the results of the comparative measurements between the present method and FIA. Both methods' final concentration of *o*-Phen was low (0.44 mmol dm^{-1}), which caused the V_d saturation due to its shortage. In contrast to the case where V_d truncated due to the instrument's measurable upper limit (see Figs. 4 and S3), the present method's advantage over FIA was limited (applicable range: 0 – 0.6 mmol dm^{-3} Fe^{2+} and 0 – 0.45 mmol dm^{-3} Fe^{2+}, respectively). This result may be due to the axial dispersion, which rounded the trapezoidal V_d waveform's corners indicated by the arrows in Fig. S8(A-2), resulting in a more significant amplitude damping.

Table 2 lists the total iron concentrations in real water samples determined by the present and the official methods [15] after reducing Fe^{3+} to Fe^{2+}. The iron level of the rusty emergency shower was in the trapezoidal profile region. The relative errors of the present method against the official method were below 10 % for any samples tested.

Conclusion

The concept of amplitude-modulated flow analysis was applied to extend the dynamic range upward to saturated signals. The flow rate of the sample solution was triangularly varied, and the obtained signal was analyzed by FFT. The quantification was based on the sum of the wave components' amplitudes ΣA. The concept was validated using aqueous solutions of Methylene Blue and colored ion complexes. Even for the saturated signal, a linear calibration curve was obtained by plotting $C_S \Sigma A$ against C_S. Although the extended range was limited due to the amplitude damping by the axial dispersion in the conduit, the present concept would provide insights for the non-dilution analysis of high concentration samples. We are extending the present concept to the saturated/truncated FIA signals for high concentration samples. The results will be reported in the near future.

Acknowledgments

The present study is partly supported by a Grant-in-Aid for Scientific Research (C) (18K05173) from the Japan Society for the Promotion of Sciences (JSPS).

Supporting Information

Derivations of Eqs. (2), (4), and (5) are described in detail. Numerical values for Figs. 3(C) and (D) are listed in Table S1. Results of the reference FIA method for MB are shown in Fig. S3. Optimization for analytical conditions for Fe^{2+} determination is shown in Fig. S4. The molar ratio method results for the Fe^{3+}–Tiron complex are shown in Fig. S5. The relationship between $C_{Fe2+} \Sigma A$ and C_{Fe2+} for trapezoidal signals obtained by *o*-Phen spectrophotometry at low *o*-Phen concentration was shown in Fig. S6. Calibration curves for Fe^{2+} determination at 2 mmol dm^{-3} *o*-Phen are shown in Fig. S7. The comparative measurements between the present

method and FIA for Fe^{2+} by *o*-Phen spectrophotometry (insufficient o-Phen system) are shown in Fig. S8. These materials are available free of charge on the Web at http://www.jsac.or.jp/analsci/.

References

[1] H. Tanaka, T. Mima, M. Takeuchi, H. Iida, Talanta, 77, 576 (2008) https://doi.org/10.1016/j.talanta.2008.03.016

[2] K. Inui, T. Uemura, T. Ogusu, M. Takeuchi, H. Tanaka, Anal. Sci. 27, 305 (2011) https://doi.org/10.2116/analsci.27.305

[3] H. Yoshida, K. Inui, M. Takeuchi, H. Tanaka, Anal. Sci. 228, 523 (2012) https://doi.org/10.2116/analsci.28.523

[4] T. Ogusu, K. Uchimoto, M. Takeuchi, H. Tanaka, Talanta, 118, 123 (2014) https://doi.org/10.1016/j.talanta.2013.10.001

[5] K. Inui, H. Yoshida, M. Takeuchi, H. Tanaka, J. Flow Inject. Anal. 2015, 32, 5 (2015) https://doi.org/10.24688/jfia.32.1_5

[6] T. Sumiomo, M. Osaki, T. Ogusu, M. Takeuchi, H. Tanaka, Anal. Sci. 33, 1363 (2017) https://doi.org/10.2116/analsci.33.1363

[7] H. Tanaka, Y. Kurokawa, M. Takeuchi, A. Ohbuchi, Talanta Open, 3, 100031 (2021) https://doi.org/10.1016/j.talo.2021.100031

[8] J. Lisec, F. Hoffmann, C. Schmitt, C. Jaeger, Anal. Chem. 88, 7487 (2016) https://doi.org/10.1021/acs.analchem.6b02515

[9] A. F. Kadjo, P. K. Dasgupta, J. Su, S. Liu, K. G. Kraiczek, Anal. Chem. 89, 3884 (2017) https://pubs.acs.org/doi/10.1021/acs.analchem.6b04857

[10] A. F. Kadjo, H. Liao, P. K. Dasgupta, K. G. Kraiczek, Anal. Chem., 89, 3983 (2017)

https://doi.org/10.1021/acs.analchem.6b04858

[11] S. Nakamura, Beginner's digital Fourier transform, (Tokyo Denki University Press, Tokyo, 1989), p. 147

[12] D. A. Skoog, F. J. Holler, S. R. Crouch, Principles of Instrumental Analysis, 7th edn. (Cengage Learning, Boston, 2018), p. 105

[13] A. Jeffrey, H.-H. Dai, Handbook of Mathematical Formulas and Integrals, 4th. edn. (Elsevier, Amsterdam, 2008) pp. 44, 45 and 283

[14] Y. Kurokawa, M. Takeuchi, H. Tanaka, Anal. Sci. 26, 791 (2010) https://doi.org/10.2116/analsci.26.791

[15] JIS K0102 Testing Method for Industrial Wastewaters (Japanese Industrial Standard Committee, Tokyo, 2013)

[16] R. Kuroda, T. Nara, K. Oguma, Analyst, 113, 1557 (1988) https://doi.org/10.1039/AN9881301557

[17] A. E. Harvey D. L. Manning, J. Am. Chem. Soc. 72, 4488 (1950) https://doi.org/10.1021/ja01166a044

[18] K. Ueno, Y. Imamura, K. L. Cheng, Handbook of Organic Analytical Reagents, 2nd edn. (CRC Press, Boca Raton, 1992), p.79

[19] W. A. E. McBryde, Can. J. Chem., 42, 1917 (1964) https://doi.org/10.1139/v64-284

Figure captions

Fig. 1 Flow system of triangular-wave controlled amplitude-modulated flow analysis. S, sample; CR, color reagent; w, waste; SG, signal generator; PC, laptop computer; $P_{1\text{-}3}$, peristaltic pumps; D, UV/Vis detector; V_c, control signal with triangular waveform; V_d, detector output signal.

Fig. 2 Principle of triangular-wave controlled amplitude-modulated flow analysis. (A) Control and analytical signals (V_c and V_d, respectively) at low analyte concentration (C_S), where V_d shows a triangular profile. (B) V_c and V_d at high C_S, where V_d shows a trapezoidal profile. (C) ΣA *vs*. Cs plot showing a linearity relationship in triangular V_d region. (D) $C_S\Sigma A$ *vs*. C_S showing linear relationship in trapezoidal V_d region.

Fig. 3 Principle of control and analytical signals (A, B) and amplitudes of wave components (C, D) for Methylene Blue (MB). Sample: 20 (A, C) and 70 (B, D) mg dm^{-3} MB. The sample flow rate was triangularly varied in the range of 0 – 1.59 cm^3 min^{-1} with a period of 120 s under a constant total flow rate of 1.61 cm min^{-1}. The P_2 channel in Fig. 1 was closed.

Fig. 4 (A) Analytical signals V_d in two periods for 0 – 100 mg dm^{-3} Methylene Blue (MB). Signals were superimposed so that they coincide in the phase. (B) Calibration curves for lower (blue) and higher (red) MB concentrations based on Eqs. (3) and (6), respectively. (C) Calibration curve for high MB concentrations based on Eq. (7).

Fig. 5 (A) Calibration curves for Fe^{2+} by *o*-Phen spectrophotometry. Sample, reagent, and total flow rate were 0 – 1.2, 0.15, and 1.47 cm^3 min^{-1}, respectively. Control period, 60 s;

reaction temperature, 50 ºC; reaction coil length, 50 cm. (B) Calibration curve for Fe^{3+} by Tiron spectrophotometry. Sample, reagent, and total flow rates were 0 – 1.2, 0.16 and 1.40 cm^3 min^{-1}, respectively. Control period, 120 s; reaction temperature, room temperature; reaction coil length, 100 cm.

Table 1. Analytical parameters

Main parameters	Values
Triangular control signal, V_c	
Scan range / V	0 − 5
Scan rate / V s^{-1}	0.166667
Period / s	60
Data acquisition and analysis	
Sampling frequency / Hz	17.06667 (10)
Number of data for FFT analysis	16
Interval of FFT analysis / s	1.875 (2)

The values in the parentheses are original values inputted by an operator. Sampling frequency and interval of FFT analysis are automatically changed to higher and shorter values than the inputted values, respectively, to be compatible with the butterfly computation algorithm in FFT.

Table 2. Determination of total iron in real water samples

Sample	C_{Fe} / mmol dm^{-3}		Ratio of A/B, %
	Present method (A)[a]	Official method (B) [b]	
Rusty shower	0.1063 ± 0.0014	0.1167 ± 0.0063	91.12
Hot spring 1	0.0301 ± 0.0008[c]	0.0303 ± 0.0017	99.27
Hot spring 2	0.0018 ± 0.0004[c]	0.0021 ± 0.0007	86.45
Matsuzakidani River	0.0046 ± 0.0014	0.0046 ± 0.0000	100.74
Hiruda Pond	0.0037 ± 0.0005[c]	0.0035 ± 0.0008	105.84

Concentrations are expressed as mean ± s.d.

[a] n = 96. The *o*-Phen concentration in the color reagent was 2 mmol dm^{-3}; [b] n = 3; [c] higher than LOD (3.3σ; 0.0015 mmol dm^{-3}) and lower than LOQ (10σ; 0.0045 mmol dm^{-3}).

Rusty shower (A) is for emergencies in the Faculty of Pharmaceutical Sciences, Tokushima University. Hot spring 1 (B) is a high-level iron-containing spring in Takarazuka, Hyogo Prefecture. Hot spring 2 (a melanterite ($FeSO_4 \cdot 7H_2O$)-containing spring) (C), the Matsuzakidani River (D), and the Hiruda Pond (E) are in Tokushima Prefecture. They were acidified with 0.2 cm^3 (Samples A, B) or 0.1 cm^3 (Samples C, D, E) sulfuric acid per 100 cm^3 sample. Each sample was filtered through an Advantec No. 131 filter paper, then twice thorough disk filter with a pore size of 0.45 μm (Kanto Chemical Co. 96904-00). 1 mL of 10 vol% hydroxyammonium chloride was added to each 100 cm^3 sample to reduce Fe^{3+} to Fe^{2+}.

Fig. 1

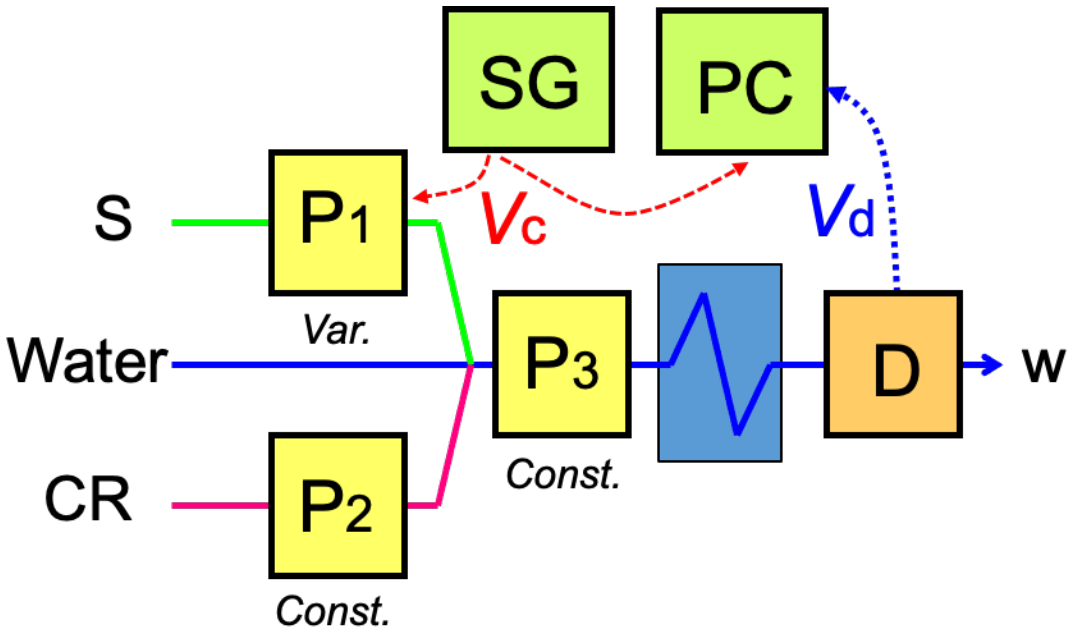

Fig. 1 Flow system of triangular-wave controlled amplitude-modulated flow analysis. S, sample; CR, color reagent; w, waste; SG, signal generator; PC, laptop computer; $P_{1\text{-}3}$, peristaltic pumps; D, UV/Vis detector; V_c, control signal with triangular waveform; V_d, detector output signal.

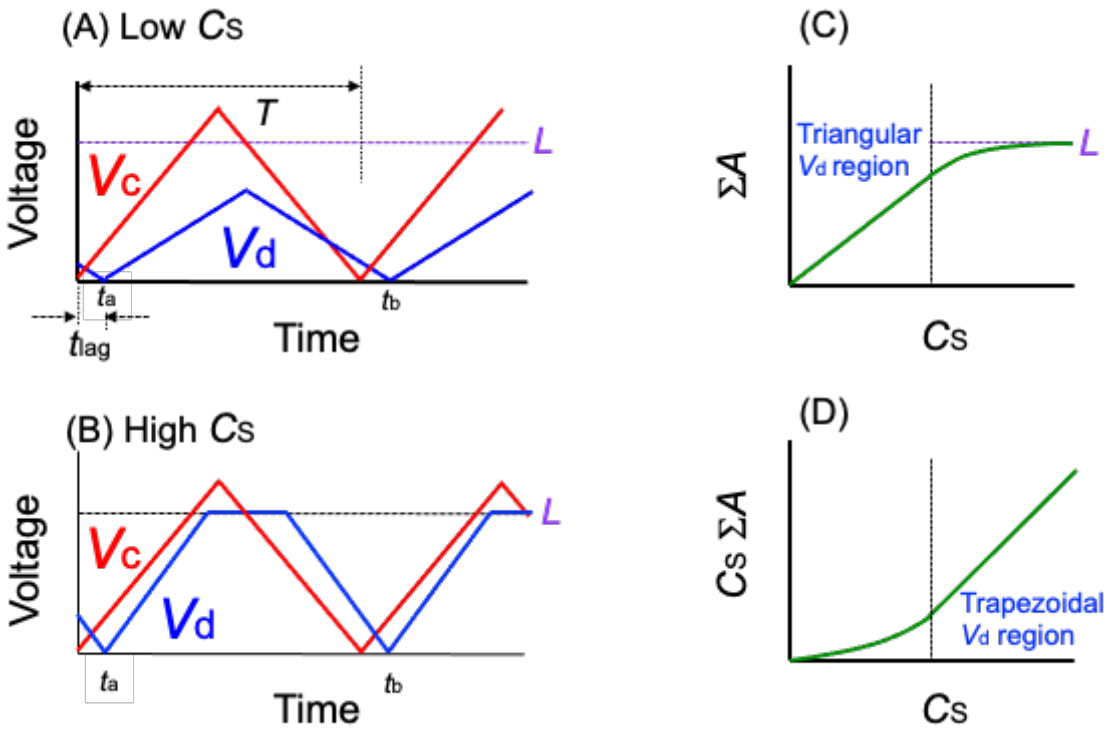

Fig. 2 Principle of triangular-wave controlled amplitude-modulated flow analysis. (A) Control and analytical signals (V_c and V_d, respectively) at low analyte concentration (C_S), where V_d shows a triangular profile. (B) V_c and V_d at high C_S, where V_d shows a trapezoidal profile. (C) ΣA *vs*. C_S plot showing a linearity relationship in triangular V_d region. (D) $C_S\Sigma A$ *vs*. C_S showing linear relationship in trapezoidal V_d region.

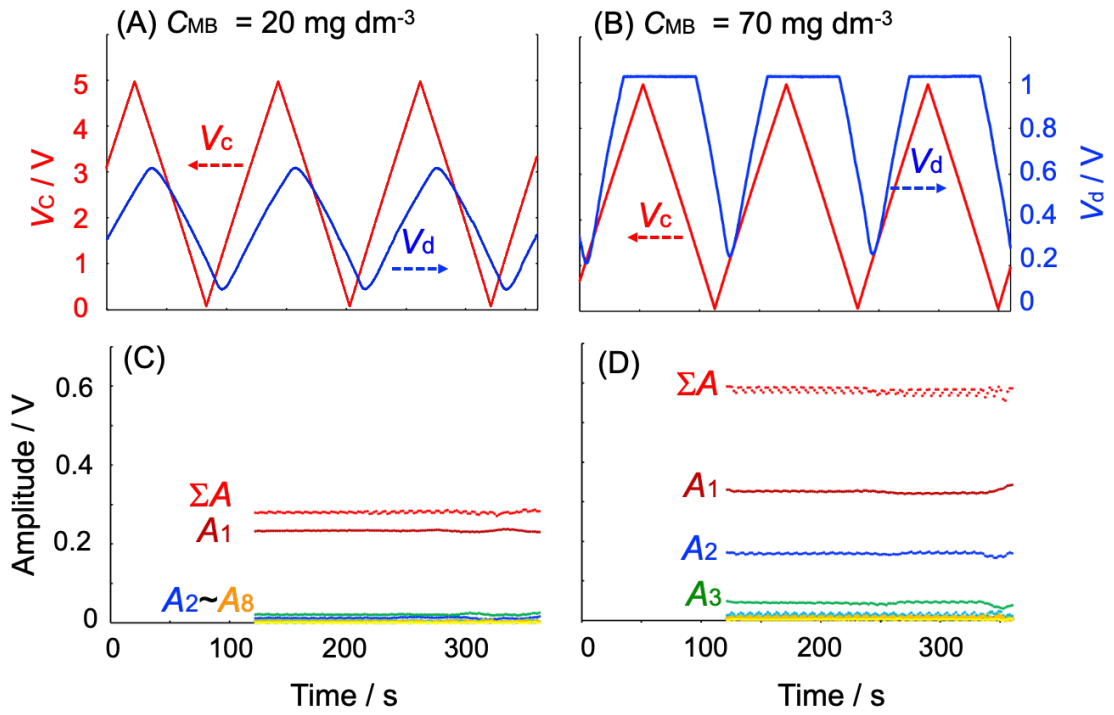

Fig. 3 Principle of control and analytical signals (A, B) and amplitudes of wave components (C, D) for Methylene Blue (MB). Sample: 20 (A, C) and 70 (B, D) mg dm^{-3} MB. The sample flow rate was triangularly varied in the range of 0 – 1.59 cm^3 min^{-1} with a period of 120 s under a constant total flow rate of 1.61 cm min^{-1}. The P_2 channel in Fig. 1 was closed.

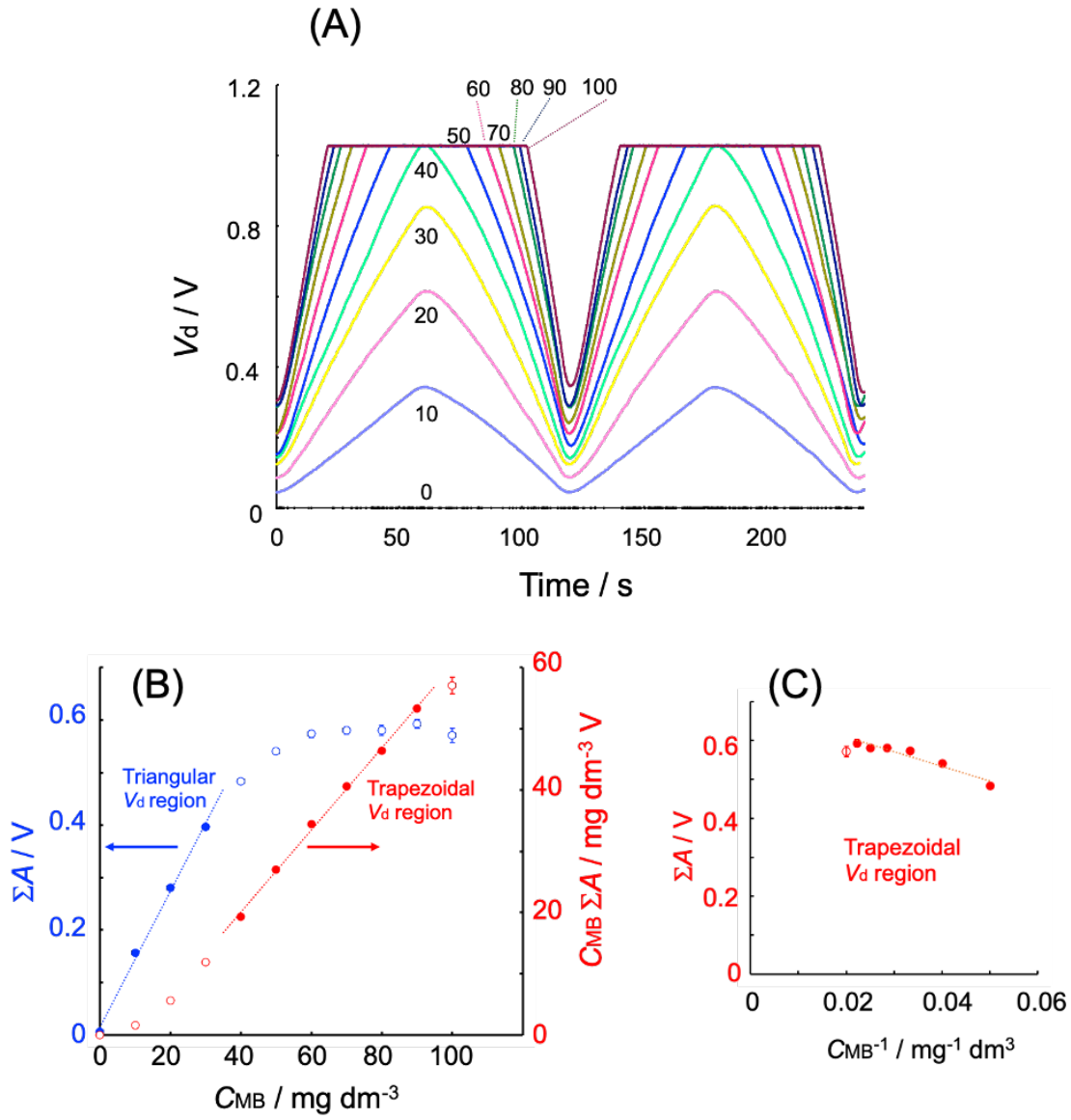

Fig. 4 (A) Analytical signals V_d in two periods for 0 – 100 mg dm^{-3} Methylene Blue (MB). Signals were superimposed so that they coincide in the phase. (B) Calibration curves for lower (blue) and higher (red) MB concentrations based on Eqs. (3) and (6), respectively. (C) Calibration curve for high MB concentrations based on Eq. (7).

Fig. 5

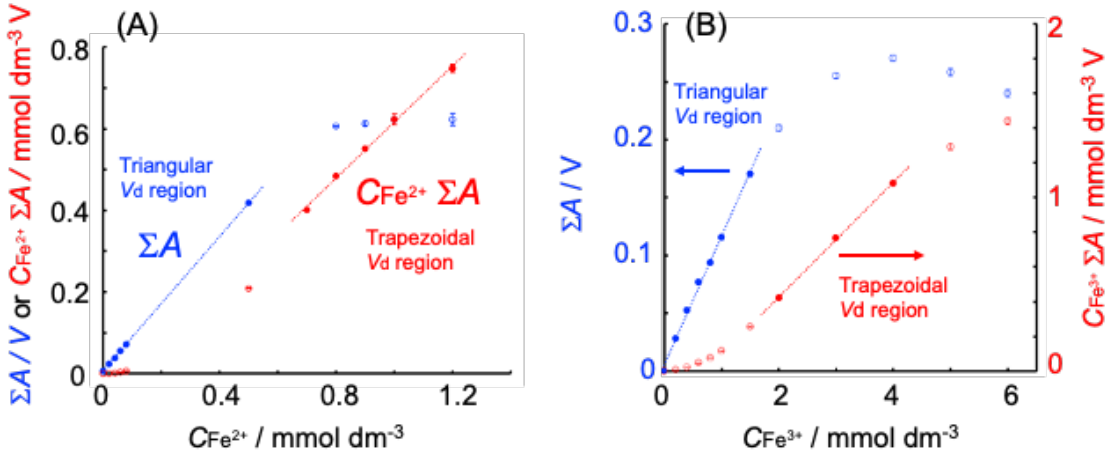

Fig. 5 (A) Calibration curves for Fe^{2+} by *o*-Phen spectrophotometry. Sample, reagent, and total flow rate were 0 – 1.2, 0.15, and 1.47 cm^3 min^{-1}, respectively. Control period, 60 s; reaction temperature, 50 ºC; reaction coil length, 50 cm. (B) Calibration curve for Fe^{3+} by Tiron spectrophotometry. Sample, reagent, and total flow rates were 0 – 1.2, 0.16 and 1.40 cm^3 min^{-1}, respectively. Control period, 120 s; reaction temperature, room temperature; reaction coil length, 100 cm.

Graphical Index